

Seismic behavior of post-tensioned precast reinforced concrete beam-to-column connections

Chin-Tung Cheng*

*Department of Construction Engineering, National Kaohsiung First University of Science & Technology,
1 University Road, Yenchao, Kaohsiung 824, Taiwan.*

(Received February 7, 2007, Accepted November 6, 2008)

Abstract. In this research, the self-centering effect in precast and prestressed reinforced concrete structures was investigated experimentally. The reinforced concrete beams and columns were precast and connected by post-tensioning tendons passing through the center of the beams as well as the panel zone of the connections. Three beam-to-interior-column connections were constructed to investigate parameters such as beam to column interfaces (steel on steel or plastic on plastic), energy dissipating devices (unbonded buckling restrained steel bars or steel angles) and the spacing of hoops in the panel zone. In addition to the self-centering effect, the shear strength in the panel zone of interior column connections was experimentally and theoretically evaluated, since the panel zone designed by current code provisions may not be conservative enough to resist the panel shear increased by the post-tensioning force.

Keywords: beam-column connections; precast; prestressed concrete; self-centering; shear distortion, large-scale testing.

1. Introduction

Capacity-designed reinforced concrete structures dissipate seismic energy through the inelastic deformation in the plastic hinge zone. Following this design, the collapse of structures can indeed be prevented, however, the accompanying damage with a large amount of residual deformation resulting in difficulty in the rehabilitation of structures after a strong earthquake. Therefore, the subject of the self-centering to minimize the permanent drift in the structures after earthquake loads has been extensively investigated recently. The concept of the self-centering was proposed by Housner (1963) who first derived the governing equations of motion for a freestanding rigid block on a rigid foundation subjected to harmonic horizontal excitations. Priestley and Tao (1993) analytically investigated the self-centering effect of precast and post-tensioned concrete structures under simulated earthquake loads. The extensive dynamic inelastic analysis showed that the displacement of a bilinear elastic system with partially bonded tendons was larger than that of a monolithic reinforced concrete connection, but not by a substantial margin.

Priestley (1996) called for joint research on what was referred to as Precast Seismic Structural System (PRESS). Prior to this research, precast structures were banned in high seismic zones due to their poor performance during earthquakes, especially in the area of beam to column connections. The objective for the PRESS research was to simulate the monolithic behavior of reinforced

* Corresponding Author, E-mail: ctcheng@ccms.nkfust.edu.tw

concrete structures in precast structures by using the post-tensioning technique. The post-tensioning technique was also applied to be the self-centering force for the bridge column in the study of Mander and Cheng (1997). The test results showed that the column behaved in a bi-linear elastic manner without severe damage or residual deformation after several cycles of 5% drift lateral loads. However, the energy dissipation of the column was limited due to its elastic performance. The energy dissipation capacity of self-centering structures was then greatly enhanced through the installation of steel angles (Ricles, *et al.* 2002) and steel rods (Christopoulos, *et al.* 2002) in the interfaces of steel beams to composite or steel columns. In addition, friction devices were also applied to dissipate seismic energy for self-centering structures such as in the research of Ricles, *et al.* (2006), Morgen and Kumura (2004) and Tsai, *et al.* (2006). It was demonstrated that the post-tensioned building systems had steady responses under cyclic loading.

Priestley and MacRae (1996) investigated the self-centering effect of a precast reinforced concrete beam-to-exterior column connection. The test results showed that the post-tensioning force in beams anchored at the column face could enhance the shear resistance of exterior column connections by providing confinement to the joint. However, in interior column joints, various anchorage configurations of post-tensioning strands may result in larger panel shear resulting in un-conservative design by current code provisions. Therefore, the objective of this research is to evaluate the shear strength in the panel zone of interior post-tensioned precast reinforced concrete beam-to-column connections by using code provisions or theoretical models, in addition to the experimental investigation of the self-centering effect. Moreover, the shear distortion behavior in the panel zone is also simulated to obtain the force-deformation relations for the connections.

2. Experimental program

Three interior reinforced beam-to-column connections were constructed and tested in the laboratory of the National Center for the Research of Earthquake Engineering (NCREE), Taiwan. In the three specimens beams and columns were all identical except for various connection details applied for each specimen. As shown in Figs. 1 and 2, the columns are 650×650 mm in size and longitudinally reinforced with 12-D36 (#11) rebars, while 8-D36 (#11) rebars for beams in the cross-section of 500×600 mm. Transverse reinforcements for columns are D13 (#4) bars with cross ties spaced at 150 mm centers outside the panel zone; but spaced at 100 or 150 mm centers without the cross-ties in the panel zone as shown in Table 1. To enhance the insufficient shear strength in the panel zone of specimen PC-A-S, an additional 15 mm thick steel plate was applied to cover the panel zone.

The investigated parameters, as shown in Table 1, include energy dissipating devices, materials in the beam-column interface, and the amount of transverse reinforcement in the panel zone. The post-tensioning strands in beams provided the restoring force, the stiffness as well as lateral load capacity for the connection. However, the connection with only post-tensioning strands may behave in a linear elastic manner with limited energy dissipation under loads. To mitigate seismic energy, supplemental energy-dissipating devices such as 2-D25 (#8) grade 75 ($f_y=517$ MPa) Dywidag bars in each of four beam slots were installed for the first two specimens (Fig. 1); while steel angles were inserted in the beam-column interface for specimen PC-A-S (Fig. 2). In Fig. 1, one end of the threaded bars was anchored at the steel plate in the beam slot by nuts, while the other was anchored inside the column through couplers. The beam slot also provided space to replace damaged threaded

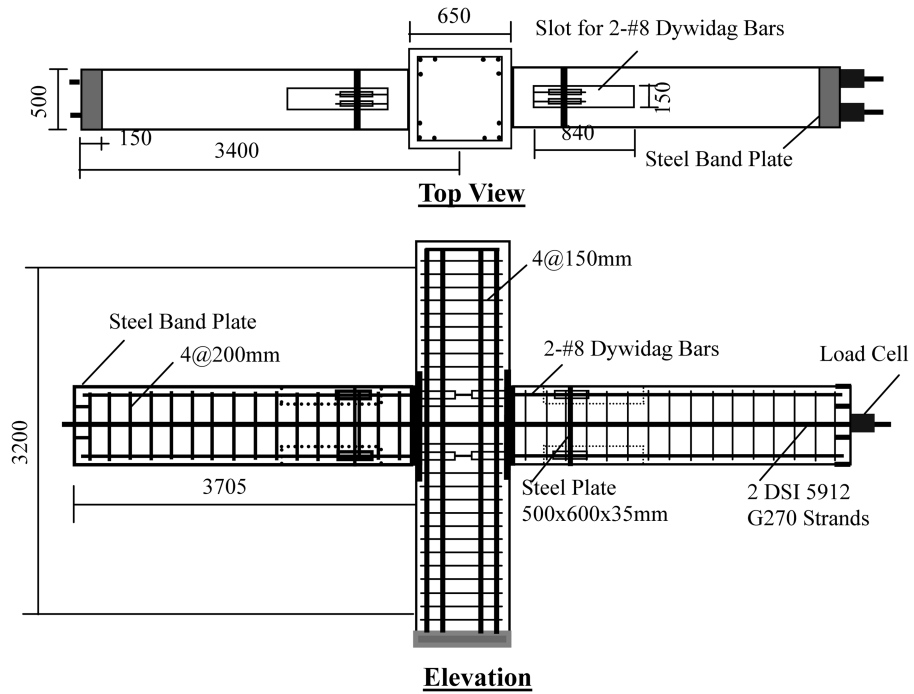


Fig. 1 Construction details for specimens PC-UB-S and PC-UB-P

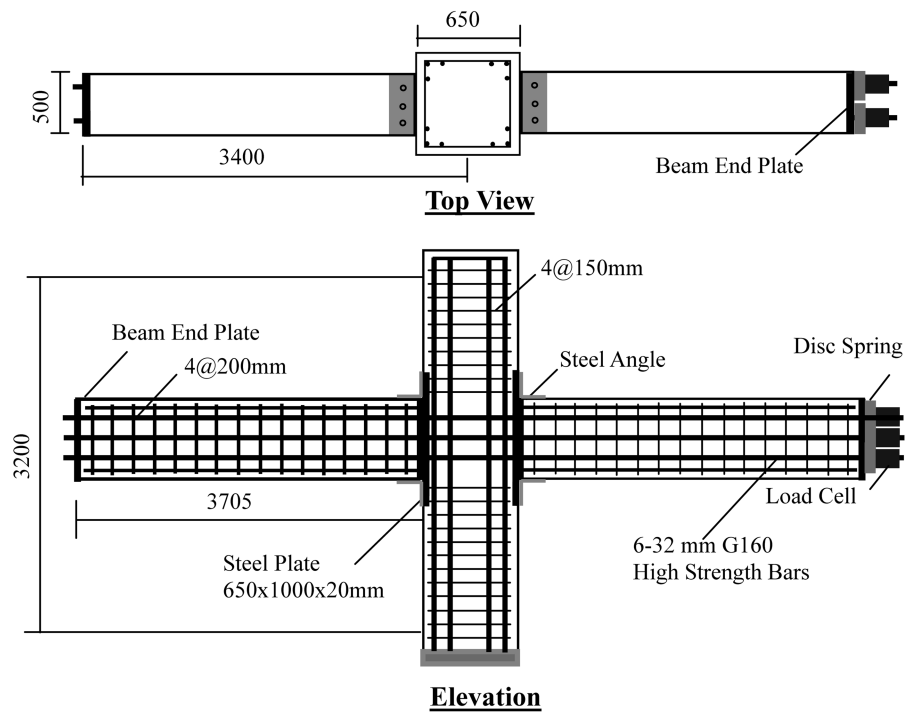


Fig. 2 Construction details for specimen PC-A-S

Table 1 Investigated parameters

Specimens	Energy Dissipation	Column Interface	Spacing of Joint Hoops	Post-Tensioned
PC-UB-S	8-D25 Dywidag Bar Grade 75	4-650×250×20 mm A36 Steel Plates	3-D13@150 mm	24-D13 (2-5912) G270 Strands
PC-UB-P	8-D25 Dywidag Bar Grade 75	2-650×800×30 mm Polyethylene Plates	5-D13@100 mm	24-D13 G270 Strands
PC-A-S	4-L200×200×20 mm A36 Steel Angles	2-650×1000×20 mm A36 Steel Plates	5-D13@100 mm 15 mm Steel Cover Plate	6-D32 G160 Tendons
Note	In specimen numbering, PC, UB, S, P and A means prestressed concrete, unbonded buckling restrained bars, steel rocking interface, Polyethylene plate interface and steel angles, respectively.			

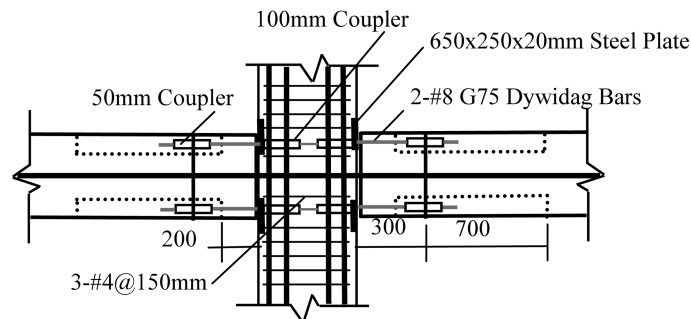
**Connection Detail**

Fig. 3 Connection details for specimen PC-UB-S

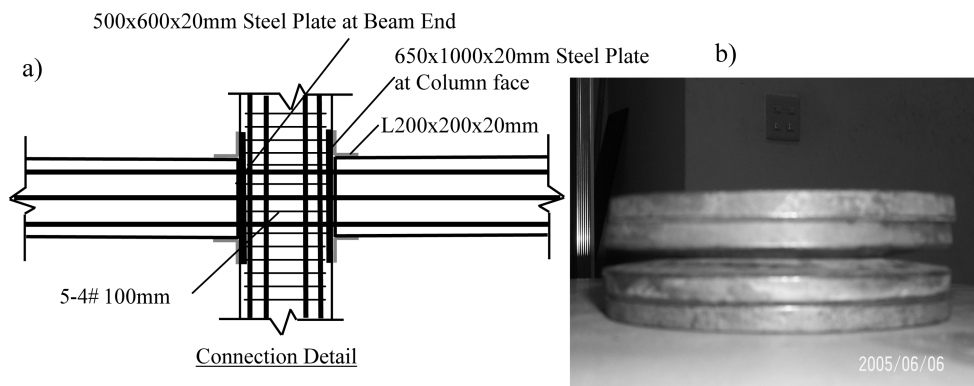


Fig. 4 Connection details and disc spring for specimen PC-A-S

bars after a strong earthquake. In the specimen PC-A-S four steel angles were installed in the corners of the beam-ends and the column face using 3-D25 A325 bolts in each angle leg.

Since the beams may rock on the column face under severe earthquake loads, the rocking toe of the beam-ends must sustain high contact pressure. To protect the cover concrete in the beam-column interface, two materials such as steel plates (Figs. 3, 4a) or Polyethylene plates were installed on the beam-ends as well as the adjacent column face. With the advantage of being lightweight and durable under extreme weather conditions and impact loads, the Polyethylene has a tensile strength

Table 2 Material properties of the steel

Components	f_y (MPa)	f_u (MPa)
D13 Rebar	412	493
D36 Rebar	480	576
Steel Angle	290	352
D25 Dywidag Bar	529	777

and elastic modulus of 25 MPa and 0.82 GPa, respectively. In steel interfaces, one plate 650×1000×20 mm in size was installed on the column face of specimen PC-A-S, while two separate plates 650×250×20 mm opposite to the rocking toe of the beam-end were applied for the specimen PC-UB-S in order to investigate the shear resistance in the panel zone. Instead of 24-13 mm G270 ($f_y=1860$ MPa) unbonded post-tensioned strands applied for the first two specimens, 6-D32 G160 ($f_y=1100$ MPa) high strength bars were used for the specimen PC-A-S so that the disc spring (Fig. 4b) could be easily installed on the anchorage zone at the beam tip. The installation of the disc spring can increase the deformation capacity of the beam under extreme lateral loads that postpones the time of yielding of high strength bars. The concrete strengths are 41 MPa, 43 MPa and 37 MPa for specimens PC-UB-S, PC-UB-P and PC-A-S, respectively. Table 2 summarizes the material strength of bars obtained from the coupon test. All reinforcing steel plates are grade A36 ($f_y=248$ MPa). The stiffness of each disc spring is 64.7 MN/m when compressed to 1.7 mm, half of the allowable displacement of the disc spring.

Fig. 5 shows the test apparatus. Before each test, the beam was post-tensioned to the total force of 1630 kN that provided 35% of the nominal moment capacity of the beam referred to as decompressed moment. When the applied moment reached decompressed moment, the gap in the beam-column interface started to open. Then, a hydraulic actuator at the top of the columns held the

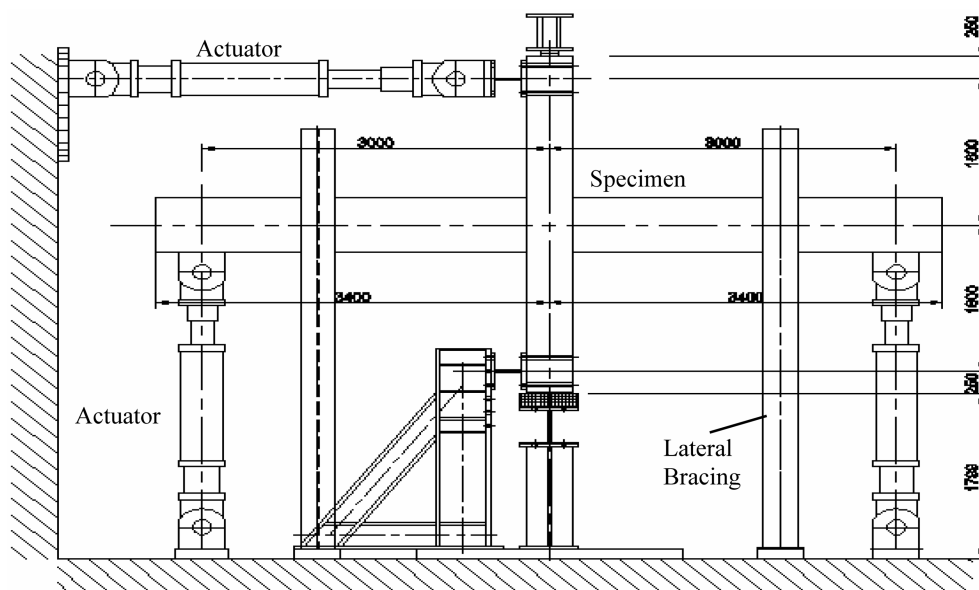


Fig. 5 Test apparatus

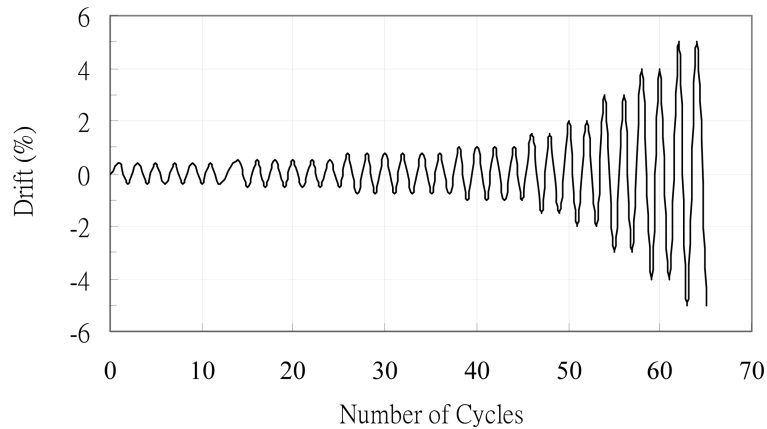


Fig. 6 Loading protocol for all specimens

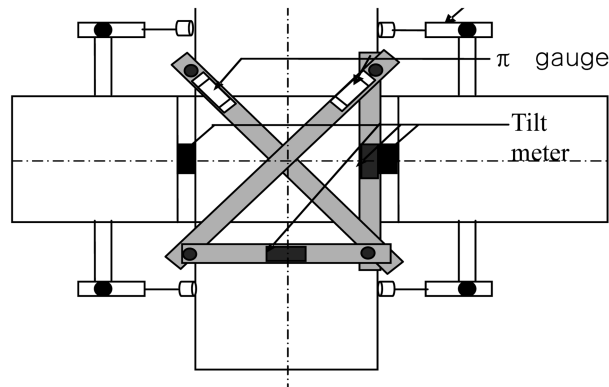


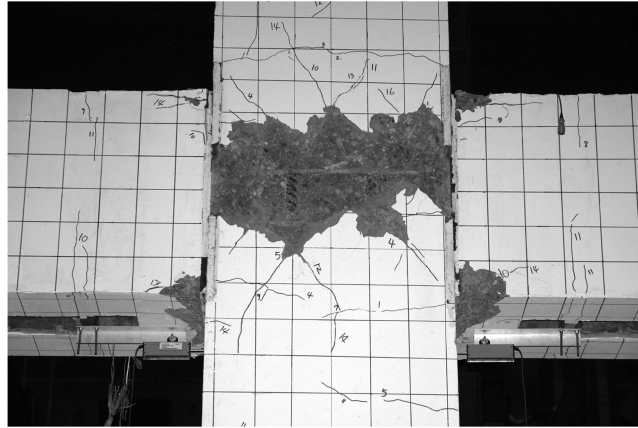
Fig. 7 Measurements in the connection

column still but allowed it to rotate. At the same time hydraulic actuators at the beam tip applied the cyclic load with displacement control in the form of triangular waves with two or three cycles at each drift increment: 0.375%, 0.5%, 0.75%, 1.0%, 1.5%, 2%, 3%, 4%, 5%, as shown in Fig. 6. The displacement rate for the tests was relatively slow and set to be constant as 1.875 mm/sec. As shown in Fig. 7, four LVDT transducers were installed at the beam-column interface for the measurement of the gap opening along with two diagonal displacement gauges in π shape for the measurement of the shear distortion in the panel zone as well as four inclinometers for the measurement of column rotation. Consequently, beam flexural deformations could be estimated by subtracting the deformations due to the column flexure, shear distortion in the panel zone, and gap opening in the beam-column interface from the total deformations measured at the beam tip in actuators.

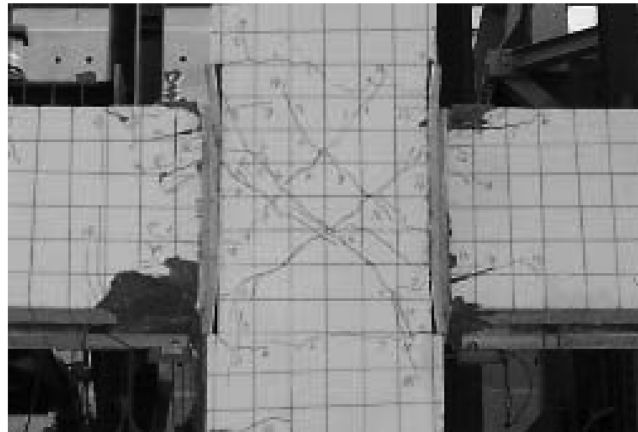
3. Test results

The visual observation revealed that the panel zone of specimen PC-UB-S failed due to panel shear in the loading of 3% drift as shown in Fig. 8a. In contrast, the panel zone of specimens PC-

(a) PC-UB-S



(b) PC-UB-P



(c) PC-A-S



Fig. 8 Photos showing the damage after each test for all specimens

UB-P and PC-A-S remained intact at all times; even though the lateral load resisting capacity of connections for the two tests deteriorated due to the spalling of beam cover concrete in the loading cycle of 3% and 4% drift, respectively. As shown in Fig. 8b, the deformed Polyethylene plate on the column face of specimen PC-UB-P due to insufficient anchorage of the plate and damaged cover concrete both significantly reduced the lever arm of the beam-end moment and panel shear transferred into the panel zone. With the reinforcement of a 15 mm thick steel cover plate as shown in Fig. 8c, the shear failure in the panel zone of specimen PC-A-S was suppressed. And the damage of the cover concrete was slightly mitigated by the confinement of steel angles at the beam-ends.

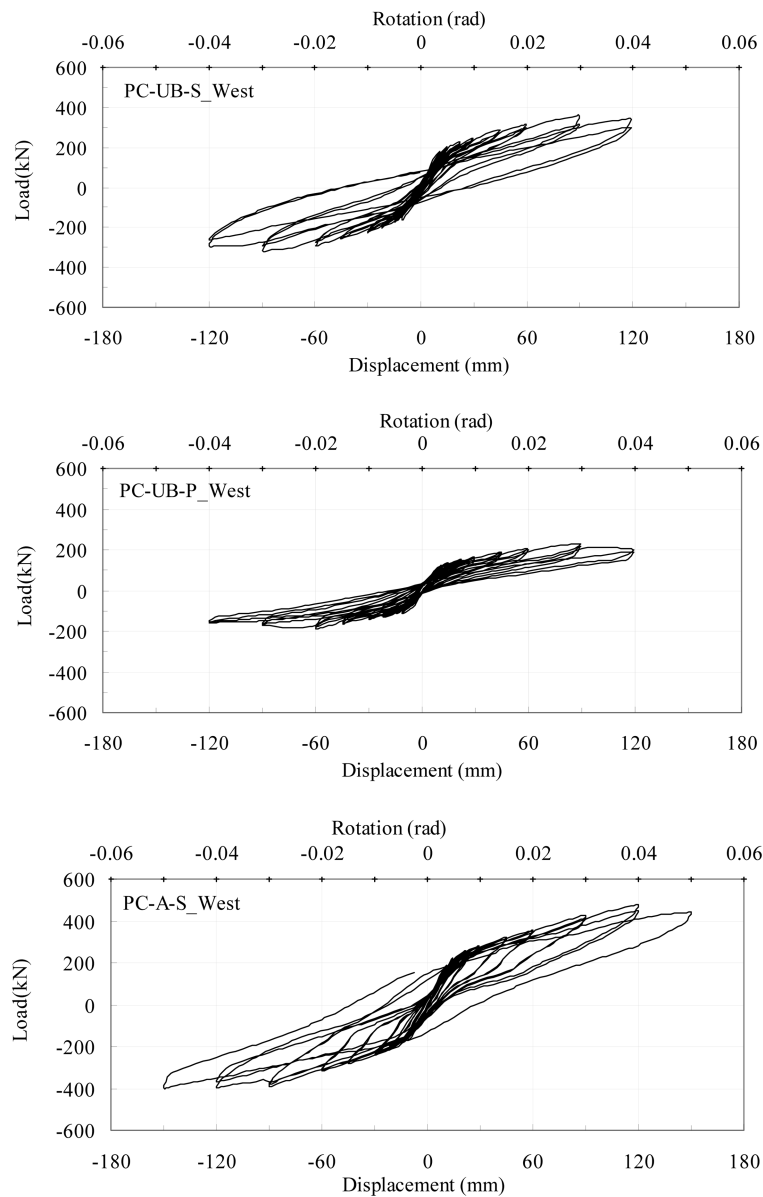


Fig. 9 Hysteretic loops in the west beam for all specimens

Both enhancing details led to much better performance in terms of the strength, ductility and residual deformation.

Hysteretic loops in the west beam for all specimens are illustrated in Fig. 9, where beam rotations were calculated with respect to the center of the columns. The self-centering effect was only observed up to a loading cycle of 2% drift for specimen PC-UB-S due to premature panel shear failure in the connection, while the self-centering effect for specimens PC-UB-P and PC-A-S was effective up to 3% and 4%, respectively. The self-centering effect was limited by the damage of the cover concrete in beam-ends afterwards. Although the hysteretic loops in specimens PC-UB-S and PC-A-S show the energy-dissipating capacity of both buckling restrained threaded bars and steel angles were satisfactory, the steel angle option may be more beneficial because of easier installation as well as replacement that can facilitate the erection of beams. The envelope of the force-deformation for all specimens is illustrated in Fig. 10 for comparison. It should be noted that the lateral load capacity of the connections increased along with the increase of drifts as the force in the post-tensioning strands increased after the gap opening, unlike conventional connections with deteriorating strength after the peak. Based on Fig. 10, the maximum moment and initial stiffness for each specimen are summarized in Table 3. It can be seen that the moment capacity of specimen PC-A-S is the largest while it is the least for specimen PC-UB-P because of the damage of the cover concrete in the beam-ends.

Total deformations in the beam tip can be decomposed into four components such as flexural deformations in the column and the beam, shear distortions in the panel zone, and gap opening in

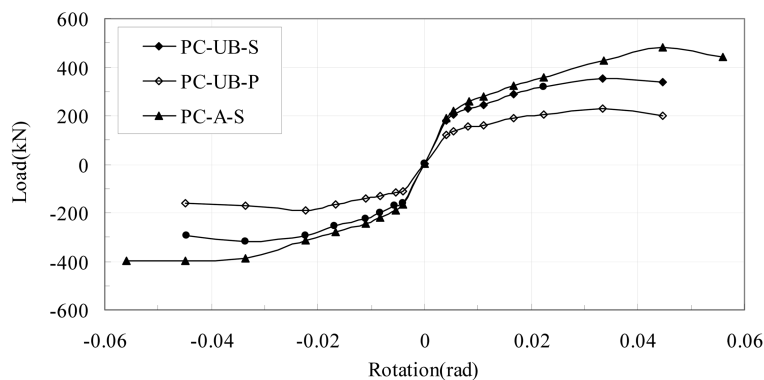


Fig. 10 Envelope of the force-deformation for all specimens

Table 3 Maximum moment and initial stiffness for all specimens

Specimens		Moment (kN-m)			Stiffness (kN-m/rad)		
		Positive	Negative	P/N	Positive	Negative	P/N
PC-UB-S	E	1000.5	952.1	1.05	133476.4	99351.5	1.34
	W	1064.1	957.0	1.11	150823.8	130647.0	1.15
PC-UB-P	E	778.9	737.0	1.06	121642.7	100806.4	1.21
	W	684.0	563.6	1.21	103306.2	90481.8	1.14
PC-A-S	E	1420.8	1273.5	1.12	175638.9	140756.6	1.25
	W	1440.0	1193.7	1.21	156332.4	137917.6	1.13

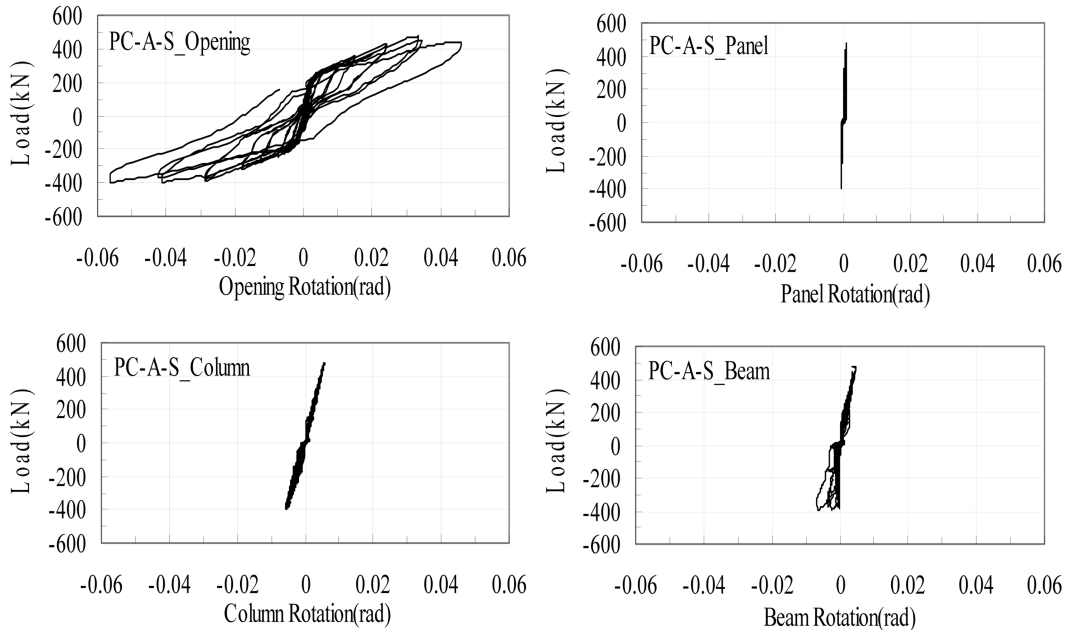


Fig. 11 Decomposition of the deformation in specimen PC-A-S

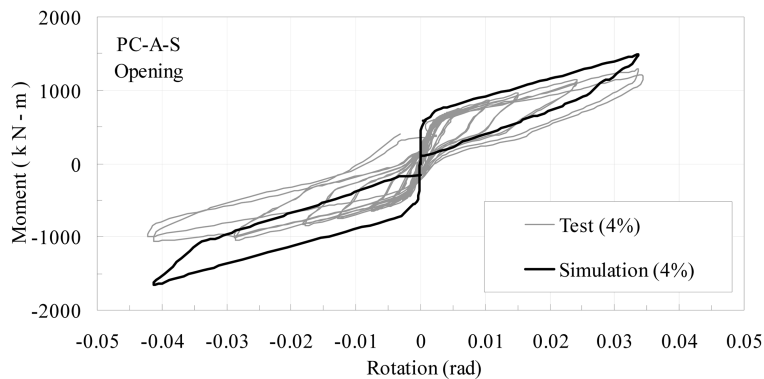


Fig. 12 Simulation of force versus gap-opening in the beam-column interface of the specimen PC-A-S

the beam-column interface. Fig. 11 shows the typical decomposition results for specimen PC-A-S. It can be seen that the gap opening accommodated the majority of deformations while the other components remained elastic up to the loading cycle of 4% drift. This performance satisfies the requirements of Taiwan code provisions for connections subjected to seismic loads. Table 4 summarizes the decomposition of deformations under the maximum load for all specimens. Since the gap opening was measured at the beam-column interface, the expression of gap opening and other deformation components as shown in Table 4 and Figs. 11-12 are all calculated with respect to the column face. This differs with the expression in Fig. 9 where beam tip rotations are calculated with respect to the center of the column. Therefore, the rotations in the Figs. 11-12 and Table 4 will be slightly larger than those presented in Fig. 9. The decomposed deformations in Table 4 show that, among the four deformation components, the gap opening ranged from 50% to 80% on

Table 4 Decomposition of deformation at beam tip under ultimate load

Specimens	Maxim Load (kN)	θ_{total} (%)	θ_{pz} (%)	θ_{open} (%)	θ_c (%)	θ_b (%)						
		(1)	(2)	(3)	(4)	(5)						
PC-UB-S	E	P	333.5	3.4	0.5	16	1.9	58	0.4	10	0.5	16
		N	317.4	3.6	0.3	11	1.6	48	0.3	10	1.1	31
	W	P	354.7	3.6	0.3	11	1.6	48	0.3	10	1.0	31
		N	319.0	3.4	0.5	16	1.9	58	0.4	10	0.5	16
PC-UB-P	E	P	259.6	3.3	0.1	3	1.7	52	0.2	6	1.3	39
		N	245.7	4.4	0.2	6	2.3	51	0.2	4	1.8	39
	W	P	228.0	3.4	0.2	6	1.6	50	0.2	7	1.2	37
		N	187.9	2.3	0.1	3	1.1	49	0.2	8	0.9	40
PC-A-S	E	P	473.6	5.1	0.1	1	4.3	80	0.6	10	0.4	9
		N	424.5	4.8	0.1	2	3.5	83	0.6	13	0.1	2
	W	P	480.0	4.2	0.1	2	3.4	75	0.6	12	0.5	11
		N	397.9	4.4	0.1	1	4.1	92	0.5	12	-0.2	-5

Note E: East Beam; W: West Beam; P: Positive Loading; N: Negative Loading

average and contained the majority of the deformations, followed by beam rotations with spalling of cover concrete in specimen PC-UB-P, the panel zone distortions in specimen PC-UB-S, and the least for the column flexural rotations in all specimens.

4. Force-deformation simulations

Since deformations in the beam tip can be decomposed into the four components (flexural deformations in the column and the beam, shear distortions in the panel zone, and gap opening in the beam-column interface), force-deformation relations for each component are simulated separately. The test results showed that the column and the beam of the connections remained elastic at all times under loads, and therefore, flexural deformations can be evaluated by the elastic beam theory using effective stiffness. Based on ACI code regulations, effective stiffness is estimated by multiplying the stiffness of the gross section for the column with axial load by 0.7 and 0.35 for the beam with extensive cracking. In this study, effective stiffness is evaluated by multiplying 0.7 for the beam with prestressing force and 0.35 for the column without axial load. The other deformation components such as the gap opening in the beam-column interface and shear distortion in the panel zone are simulated in the following sections.

4.1. Gap-opening in the beam-column interface

When the gap open, post-tensioning tendons and energy dissipating steel angles or buckling restrained bars deform according to the geometry. Based on the research of Christopoulos, *et al.*

2002, tensile strain in the post-tensioning tendons increased by the gap opening, θ , can be modified by adding the softening effect, α_{PT} , to account for the installation of the disc spring at the beam-tip and expressed as:

$$\varepsilon_{PT} = \varepsilon_o + \left[\frac{\alpha_{PT}(d_{PT} - a_b)}{L_{PT}} \right] \left(1 - \frac{A_{PT}}{A_b} \right) \quad (1a)$$

and the tensile strain in the energy dissipating devices is:

$$\varepsilon_{ED} = \left[\frac{(d_{ED} - a_b)\theta}{L_{ED}} \right] \quad (1b)$$

where ε_o and ε_{PT} are the strains in the post-tensioning tendons prior to and after the gap opening. L_{PT} and A_{PT} are the anchored length and cross-section area of post-tensioning tendons, respectively. A_b is the cross-section area of the beam, and the ratio of A_{PT}/A_b in Eq. (1) accounts for the beam shortening due to the post-tensioning force. d_{PT} and d_{ED} are the height of post-tensioning tendons and energy dissipating devices with respect to the rocking toe of the beam. ε_{ED} and L_{ED} are the strain and anchored length of the energy dissipating devices. Since post-tensioning tendons first compresses the disc spring then the beam at the anchorage zone of the beam tip, α_{PT} is a fraction of the axial flexibility of post-tensioning tendons to the total flexibility including the disc spring. The depth of the neutral axis in the beam, a_b , can be estimated by the recommendations of Paulay and Priestley (1992) as:

$$a_b = \left(0.25 + 0.85 \frac{P}{A_b f'_c} \right) d_b \quad (2)$$

where P is the prestressing force provided for the beams, and d_b and f'_c are the depth and concrete strength of the beam, respectively. Based on the stress-strain curve of the post-tensioning tendons, the restoring force increased along with the gap opening can be obtained from the strain increase in Eq. (1a).

Similarly, the strain increase in the energy dissipating devices such as steel angles or buckling restrained bars can be calculated using Eq. (1b). Based on the stress-strain relationship of the materials, the restoring force in the energy dissipating devices can also be obtained. For example, the restoring force in steel angles may be evaluated through the research of Ricles, *et al.* (2002) as:

$$V_a = \beta \frac{2M_{pa}}{g} \quad (3)$$

where β is the over-strength factor, M_{pa} is the plastic moment of the steel angle, and g is the gauge length of an angle leg. Therefore, the resisting moment in beams can be calculated as:

$$M_b = \sum_{i=1}^n A_{PTi} f_{PTi} d_{PTi} + \sum_{i=1}^n V_{ai} d_{ai} \quad (4)$$

where f_{PTi} is the tensile stress in the post-tensioning tendons and V_{ai} is the force in the steel angles. d_{PTi} and d_{ai} represent the height of the post-tensioning tendons and steel angles with respect to the rocking toe of the beam, respectively. Test results showed that only specimen PC-A-S exhibited satisfactory self-centering effects. The force-gap opening relations of the specimen are illustrated in Fig. 12. It can be seen that the simulated curve agrees well with the test results; however, there is a little deviation in the pull direction (negative rotation) of the curve resulting from the concrete

crushing in the beam corner.

4.2. Shear distortions in the panel zone

The shear capacity and distortion behavior in the panel zone of the connections are evaluated by the following theory. When the connection is subjected to the panel shear as shown in Fig. 13, a diagonal concrete strut will be formed to transmit the panel shear. The strut area can be estimated by the depth of the beam compression zone (Eq. 2). Due to the panel distortion, the diagonal concrete strut is shortened and compressed, while it is simultaneously tensioned in the orthogonal direction. Based on the deformed relation between points in the panel zone as illustrated in Fig. 14, compressive strain in the concrete strut, ε_c , due to the panel distortion, γ , can be calculated as:

$$\varepsilon_c = \frac{\sqrt{(l_{BC} - l_{AB} \cdot \gamma)^2 + l_{AB}^2} - l_{AC}}{l_{AC}} \quad (5)$$

Similarly tensile strain perpendicular to the diagonal strut, ε_t , can be calculated as:

$$\varepsilon_t = \frac{\sqrt{(l_{DC} \cdot \gamma + l_{BC})^2 + l_{DC}^2} - l_{BD}}{l_{BD}} \quad (6)$$

where $l_{DC} = \frac{l_{BD}^2}{l_{AB}}$, l_{BC} , l_{AC} , l_{BD} represent the distances between points in the panel zone as shown in Fig. 14, respectively. To simulate the deformation behavior of the strut concrete, a confined stress-strain model proposed by Mander, *et al.* (1988) is modified by adding the softening effect, ζ , due to the orthogonal tension as:

$$f_c = \frac{\zeta f_{cc} x r}{r - 1 + x^r} \quad (7)$$

where, $x = \frac{\varepsilon_c}{\zeta \varepsilon_{cc}}$, $r = \frac{E_c}{E_c - E_{sec}}$; and E_c is the Young's Modulus of the concrete, E_{sec} the secant modulus of the concrete, ε_c the concrete strain corresponding to f_c , ε_{cc} the confined concrete strain corresponding to f_{cc} , and f_{cc} the confined concrete strength on the basis of Mander, *et al.* (1988) to be

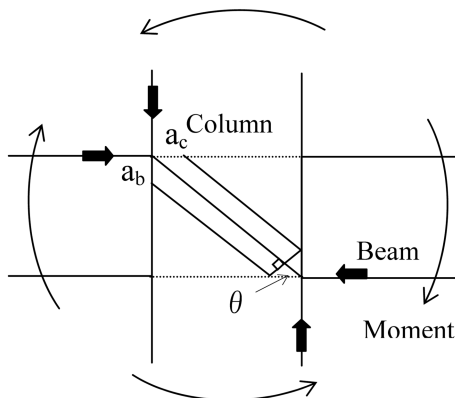


Fig. 13 Concrete struts in the panel zone

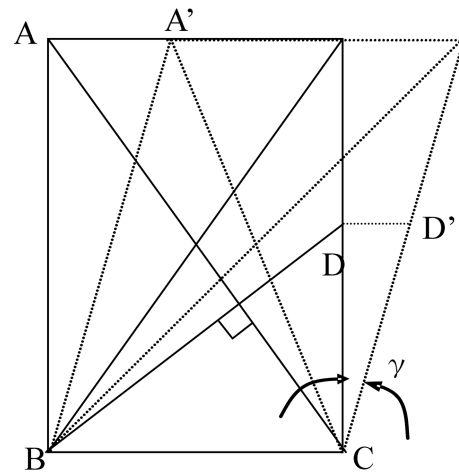


Fig. 14 Shear distortions in the panel zone

$$f_{cc} = f'_c \left(-1.254 + 2.254 \sqrt{1 + \frac{7.94f_l}{f'_c}} - 2 \frac{f_l}{f'_c} \right) \quad (8)$$

where f_l is the confining stress provided by the stirrups. In estimating the confinement in the panel zone of specimen PC-A-S, the cover steel plate is assumed to be a continuous stirrup. In addition to the compression, the strut concrete is also tensioned in the orthogonal direction, which results in the softening of the compressive strength of the strut concrete. On the basis of the research by Zhang and Hsu (1998), the softening coefficient may be estimated by replacing the term of unconfined concrete strength with confined concrete strength as:

$$\zeta = \frac{5.8}{\sqrt{f_{cc}}} \frac{1}{\sqrt{1 + 400 \varepsilon_t}} \leq \frac{0.9}{\sqrt{1 + 400 \varepsilon_t}} \quad (9)$$

where the unit of f_{cc} is MPa. The angle of the diagonal concrete strut is defined as:

$$\theta = \tan^{-1} \left(\frac{d_b}{d_c} \right) \quad (10)$$

where d_b is the beam depth and d_c the column depth in the lateral loading direction. Therefore, the strut area in the diagonal direction is calculated as:

$$A_{str} = b_c \frac{a_b}{\cos \theta} \quad (11)$$

where b_c is the column width. Then, the panel shear resisted by the concrete strut can be expressed as:

$$V_n = f_c A_{str} \cos \theta = f_c a_b b_c \quad (12)$$

In specimen PC-A-S, since the panel zone was reinforced with a 15 mm thick steel cover plate, the shear strength contributed by the concrete strut and steel cover plate in the panel zone should be superposed. The shear strength of the steel plate can be estimated in an elastically perfectly plastic manner as:

$$V_{sp} = \frac{f_y}{\sqrt{3}} A_{sw} \quad (13)$$

where f_y and A_{sw} are the tensile strength and the web area of the steel cover plate, respectively.

In addition to the above theoretical approach, the shear strength in the panel zone can also be evaluated by ACI 318-2005 code regulations as well as a softened strut and tie model proposed by Hwang and Lee (2002). Based on the ACI code provision, the shear strength of the connections can be estimated as:

$$V_n = 1.25 \sqrt{f'_c} A_j \quad (MPa) \quad (14)$$

where f'_c is the concrete strength and A_j the effective joint area deducting the hole area for the unbonded post-tensioning strands. In contrast, the softened strut and tie model proposed by Hwang and Lee (2002) calculated the shear strength of the joint as:

$$V_n = C_{d,n} \cos \theta \quad (15)$$

$$C_{d,n} = (K_h + K_v - 1) \cdot \zeta \cdot f'_c \cdot A_{str} \quad (16)$$

Table 5 Analytical shear strength and test results in the panel zone

Specimens	Tested Loads (kN)	Analytical Shear Strength			Failure Mode
		ACI (kN)	H & L (kN)	Proposed (kN)	
PC-UB-S	2730	2335	2424	2687	shear
PC-UB-P	1823	2402	2535	2750	-
PC-A-S	3637	4102	3664	6211	-

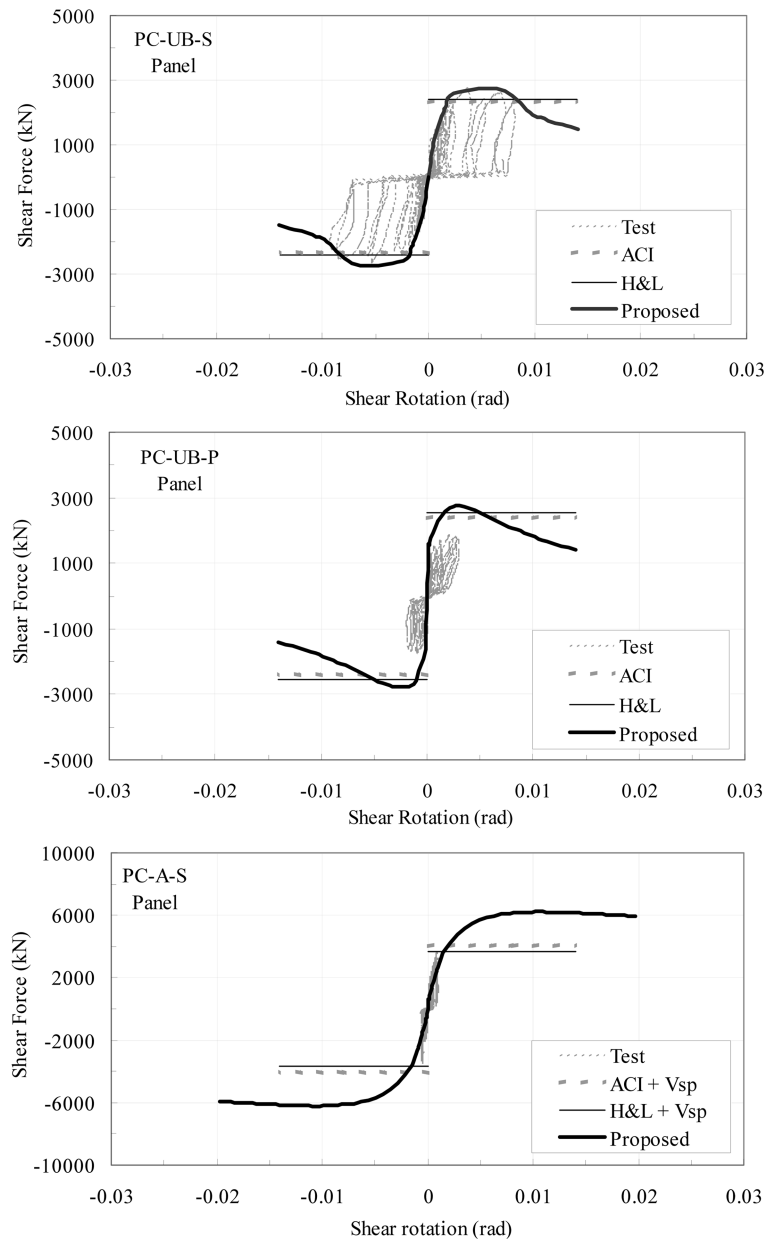


Fig. 15 Analytical and experimental panel shear versus rotation at the beam tip

where ζ is the softening coefficient, A_{str} the strut area, and K_h and K_v the indices for the amount of horizontal and vertical tie provided for the joint, respectively.

Table 5 summarizes analytical shear strength in the panel zone and compared with test results for all specimens. Fig. 15 illustrates the analytical shear capacity and the distortion behavior along with test results for all specimens. It can be seen that the proposed model not only can evaluate the shear strength in the panel zone comparable to existing models, but also can simulate the distortion behavior. As shown in Table 5, the tested panel shear in specimen PC-UB-S is larger than all the predicted strengths. This indicates the inappropriateness of the current code provisions in designing the joint. Current code provisions fail to account for the increase of panel shear due to the post-tensioning force for interior column connections. In contrast, tested panel shear in specimens PC-UB-P and PC-A-S is less than the predicted strengths, indicating that the panel zone remained intact without premature failure as shown in the test. It is noted that the shear capacity predicted by three analytical models for specimen PC-A-S include the contribution of steel cover plate by using Eq. (13).

It can be seen from Fig. 15 that the shear distortion behavior in the panel zone of specimen PC-UB-S is well simulated by the proposed theory, while it is overestimated for specimen PC-UB-P, as its tested panel shear was significantly reduced by the damage of the cover concrete in the beam ends. In this specimen, slight plasticity in the hysteretic loops is attributed to the diagonal cracks that developed in the panel zone during tests as shown in Fig. 8b. On the other hand, the elastic performance in the panel zone of specimen PC-A-S indicates the conservative prediction of the shear strength by the two existing models since they neglect the confinement of steel cover plate to the panel zone.

4.3. Force-deformations of entire sub-assembly

Since the deformation at the beam-tip can be decomposed into the four components, force-deformation relations of the connection can be theoretically simulated by firstly assuming a similar gap opening in each beam end. Then, the corresponding beam-end moments, positive in one end and negative in the other, can be obtained on the basis of the derived force versus gap-opening relationship. Based on these beam-end moments, component deformations such as flexural rotations in the column and beams as well as panel distortions can be theoretically estimated. Therefore, total deformation at the beam tip is simulated by superposing by the deformation of the four components corresponding to these beam-end moments. This procedure is repeated by assuming a new gap opening in each beam-end. Finally, the envelope of the force-deformation for the connections can be estimated and compared with tested hysteretic loops as shown in Fig. 16. It can be seen that the simulations agree well with the test results except for specimen PC-UB-P where beam-end moments were significantly reduced because of the damage of cover concrete that was not considered in the theory. It is also noted that the proposed theory is incapable of simulating hysteretic behavior of shear strength versus distortion in the panel zone. For this reason, the envelope of force-deformation relation was simulated for the first two specimens rather than the hysteretic loops, since they failed due to the panel shear in the connection or the spalling of cover concrete in the beam that should be suppressed in the practical design.

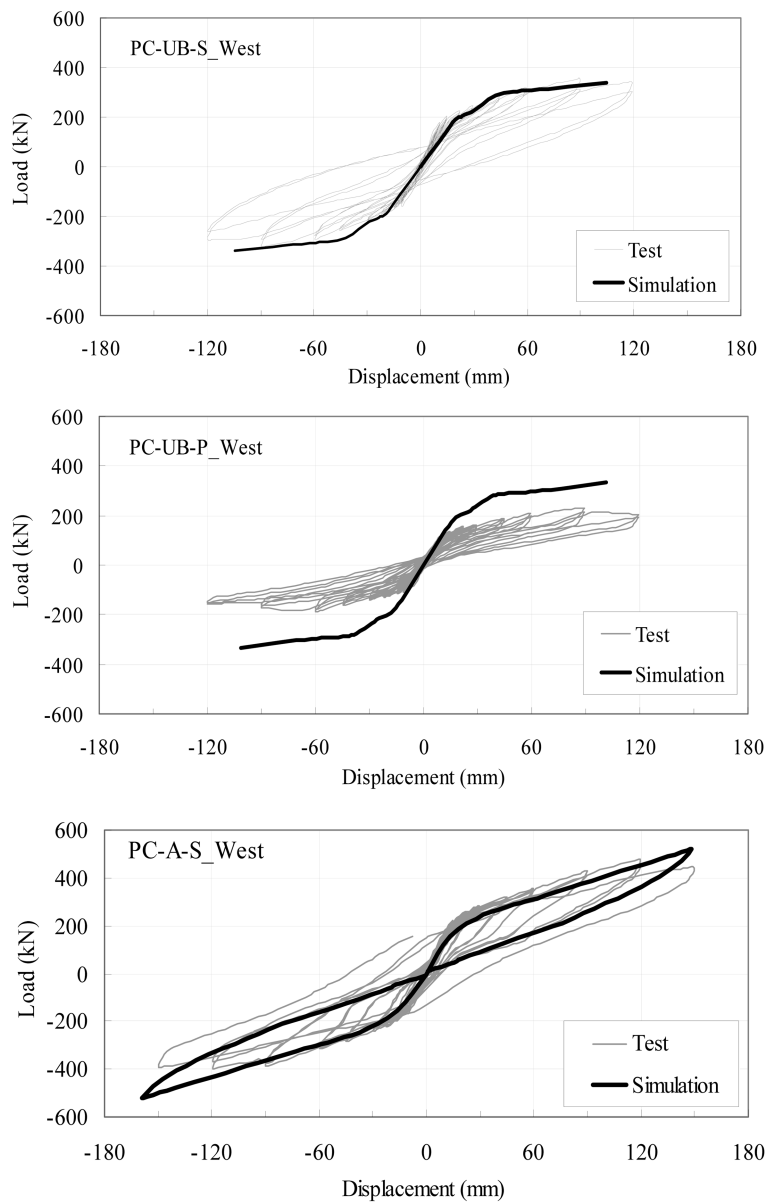


Fig. 16 Force-deformation simulations for the entire connection of all specimens

5. Conclusions

Based on the experimental results and analytical evaluation of the tests, the following conclusions can be drawn:

1. The post-tensioned reinforced concrete beam-column connection with a steel-on-steel interface, steel cover plate in the panel zone, and steel angles as energy-dissipating devices had the best performance in terms of effective self-centering function up to the loading of 4% drift.
2. As energy-dissipating devices, steel angles are a better choice than buckling restrained bars

because of easier installation and replacement, which facilitates the erection process, in addition to the mitigation of the damage of cover concrete at the beam end.

3. The deformation of self-centering connections can be decomposed into four components, in which the gap opening accommodates the majority of the deformation, followed by the beam rotations and shear distortions in the panel zone, and the column flexural rotations. The proposed model not only evaluates the shear strength of the connections but also simulates the gap-opening behavior, shear distortion relations and even the force versus total deformation relations of the connections.

4. Test results in the literature showed that the post-tensioning force could enhance the shear resisting capacity in the panel zone of the exterior beam-column connections. In contrast, the test results in this research revealed that the post-tensioning force also increased the panel shear of the interior beam-column connections, leading to an un-conservative design by the current code provisions or existing models. If the panel zone was covered by a steel plate, both the code provisions and existing models significantly underestimated the shear resisting capacity of the specimen, since they ignored its confinement effect to the strut concrete.

5. In practice, floor slabs are designed in a way of rigid diaphragm that may limit the gap opening in the beam-column interface. The stiffness of the slab may be too stiff to open the gap in the beam-column interface, or too soft to transfer the seismic loads from the gravity frame to the moment-resisting frame. Therefore, the design of the floor slab will be critical for self-centering structures and needs to be investigated further.

6. Nomenclature

A_b	gross area of beam cross-section;
A_j	effective joint area;
A_{PT}	total area of post-tensioning strands in beams;
A_{str}	area of diagonal concrete strut;
A_{sw}	web area of the steel cover plate;
a_b	depth of the compression zone in beams adjacent to the joint;
a_c	depth of the compression zone in columns adjacent to the joint;
b_c	column width in the loading direction;
$C_{d,n}$	axial force of diagonal concrete strut in the panel zone;
d_a	distance between the steel angle and rocking toe in beams;
d_b	beam depth in the loading direction;
d_c	column depth in the loading direction;
d_{PT}	distance between post-tensioning tendons and rocking toe in beams;
E_c	Young's modulus of the concrete;
E_{sec}	secant modulus of the concrete;
f_c	compressive strength of the strut concrete in the panel zone;
f_{cc}	confined strength of the strut concrete in the panel zone;
f_l	confining pressure to the strut concrete from the stirrup;
f_{PT}	tensile strength in the post-tensioning strands;
f_u	tensile strength of the steel;
f_y	yield strength of the steel;
g	gauge length of the angle leg;

γ	panel distortion
K_h	index for the horizontal tie provided in the joint;
K_v	index for the vertical tie provided in the joint;
l_{AB}	distance between the points A and B in the panel zone;
l_{AC}	distance between the points A and C in the panel zone;
l_{CD}	distance between the points C and D in the panel zone;
l_{BC}	distance between the points B and C in the panel zone;
l_{BD}	distance between the points B and D in the panel zone;
M_{pa}	plastic strength of steel angles;
P	prestressing force in beams;
r	coefficient controlling the post-peak behavior of stress-strain curve for the strut concrete;
V_a	tensile force resisted by steel angles;
V_n	nominal shear strength in the panel zone;
V_{sp}	shear strength of the steel cover plate;
α_{PT}	softening factor of the axial flexibility of the post-tensioning strands because of the disc spring;
β	over-strength factor of the steel angles;
ϵ_c	compressive strain in the strut concrete corresponding to f_c ;
ϵ_{cc}	confined strain in the strut concrete corresponding to f_{cc} ;
ϵ_o	initial strain in the post-tensioning tendons;
ϵ_{PT}	strain in the post-tensioning tendons after gap opened;
ϵ_i	tensile strain perpendicular to the diagonal strut;
ζ	softening coefficient in the stress-strain curve of the strut concrete;
θ	angle of the concrete strut with respect to the horizontal in the panel zone
γ	panel distortion.

Acknowledgments

Financial support from the National Science Council in Taiwan through grant No. NSC93-2625-Z-001 is greatly appreciated. In addition, technical help from the laboratory at the NCREE, Taiwan is also acknowledged. The author would also like to thank Mr. C-T. Liu for his assistance in experiments.

References

- ACI Committee 318-2005. *Building Code Requirement for Structural Concrete and Commentary*, American Concrete Institute, Mich., USA.
- Christopoulos, C., Filiatraut, F., Uang, C.M. and Folz, B. (2002) "Post-tensioned energy dissipating connections for moment resisting steel frames," *J. Struct. Eng., ASCE*, **128**(9), pp. 1111-1120.
- Housner, G.W. (1963) "The behavior of inverted pendulum structures during earthquakes," *Bulletin of the Seismological Society of American*; **53**(2), pp. 403-417.
- Hwang, S.J. and Lee, H.J. (2002) "Strength prediction for discontinuity regions by softened strut and tie model," *J. Struct. Eng., ASCE*, **128**(12), pp. 1519-1526.
- Mander, J.B., Priestley, M.J.N. and Park, R. (1988) "Theoretical stress-strain model for confined concrete," *J. Struct. Eng., ASCE*, **114**(8), pp. 1804-1826.
- Mander, J.B. and Cheng, C-T. (1997) "Seismic resistance of bridge piers based on damage avoidance design,"

- Technical Report NCEER 97-0014; Buffalo, NY.
- Morgen, GB. and Kumara, Y.C. (2004) "A friction damper for post-tensioned precast concrete beam-to-column joints," 13th World Conference on Earthquake Engineering, Vancouver, Canada, Aug. 1-6, 2004, Paper No. 3189.
- Paulay, T. and Priestley, M.J.N. (1992) *Seismic Design of Reinforced Concrete and Masonry Buildings*. John Wiley & Sons, p. 274.
- Priestley, M.J.N. (1996) "The PRESS program—current status and proposed plans for phase III," *PCI J.*, **41**(3), pp. 22-40.
- Priestley, M.J.N. and MacRae, G.A. (1996) "Seismic testing of precast beam-to-column joint assemblages with unbonded tendons," *PCI J.*, **41**(1), pp. 64-80.
- Priestley, M.J.N. and Tao, J.R. (1993) "Seismic response of precast prestressed concrete frames with partially debonded tendons," *PCI J.*, **38**(1), pp. 58-66.
- Ricles, J.M., Sause, R., Peng, S.W. and Lu, L.W. (2002) "Experimental evaluation of earthquake resistant post-tensioned steel connections." *J. Struct. Eng., ASCE*, **128**(7), pp. 850-859.
- Ricles, J.M., Sause, R., Wolski, M., Seo, C.Y. and Iyama, J. (2006) "Experimental behavior of a self-centering steel moment connection with a bottom flange friction device", US-Taiwan workshop on self-centering structural systems 2006, edited by Tsai, K.C. and Ricles, J.M., National Center on the Research of Earthquake Engineering, Technical Report No. 06-013, October 14, 2006, Taipei, Taiwan, pp. 5-8.
- Tsai, K.C. Chou, C.C., Lin, C.L. Chen, P.L. and Jhuang, S.J. (2006) "Seismic self-centering steel beam-to-column connections using bolted web friction devices", US-Taiwan workshop on self-centering structural systems 2006, edited by Tsai, K.C. and Ricles, J.M., National Center on the Research of Earthquake Engineering, Technical Report No. 06-013, October 14, 2006, Taipei, Taiwan, pp. 12-13.
- Zhang, L.X.B. and Hsu, T.T.C. (1998) "Behavior and analysis of 100 MPa concrete membrane elements," *J. Struct. Eng., ASCE*, **124**(1), pp. 24-34.